京都大学学術情報リポジトリ
KURENAI 紅
Kyoto University Research Information Repository

京都大学
KYOTO UNIVERSITY

Title	Structures of dayside whistler-mode waves deduced from conjugate diffuse aurora
Author(s)	Nishimura, Y.; Bortnik, J.; Li, W.; Thorne, R. M.; Ni, B.; Lyons, L. R.; Angelopoulos, V.; Ebihara, Y.; Bonnell, J. W.; Le Contel, O.; Auster, U.
Citation	Journal of Geophysical Research: Space Physics (2013), 118(2): 664-673
Issue Date	2013-02
URL	http://hdl.handle.net/2433/193718
Right	©2012. American Geophysical Union.
Type	Journal Article
Textversion	publisher

Kyoto University

JOURNAL OF GEOPHYSICAL RESEARCH: SPACE PHYSICS, VOL. 118, 664–673, doi:10.1029/2012JA018242, 2013

Structures of dayside whistler-mode waves deduced from conjugate diffuse aurora

Y. Nishimura,[1] J. Bortnik,[1] W. Li,[1] R. M. Thorne,[1] B. Ni,[1] L. R. Lyons,[1]
V. Angelopoulos,[2] Y. Ebihara,[3] J. W. Bonnell,[4] O. Le Contel,[5] and U. Auster[6]

Received 28 August 2012; revised 15 October 2012; accepted 2 November 2012; published 11 February 2013.

[1] We present simultaneous measurements of dayside diffuse aurora and whistler-mode waves made by the South Pole all-sky imager and two of the THEMIS spacecraft. We found a high correlation between the diffuse aurora intensity at 557.7 nm near the footprint latitudes of THEMIS and whistler-mode wave intensity measured on board. The power in other wave modes was negligibly small in most cases, indicating that the dayside diffuse aurora is driven by precipitating energetic electrons resonating with whistler-mode waves. The high correlation over a wide L^* range ($6 < L^* < 11$) further allowed us to magnetically link the wave and magnetospheric plasma distributions with the auroral patterns. Two distinct regions of whistler-mode waves and ambient plasma density were found outside the plasmasphere near the equator: (1) intense waves in a smooth, low density and (2) moderate waves with enhanced and fluctuating density. The whistler-mode wave intensity in the fluctuating plasma density region is positively correlated with the ambient density variations. The corresponding auroral images show an azimuthally elongated diffuse auroral band on the field lines connected to the low density region, as opposed to a structured diffuse aurora on the fluctuating density field lines. Each structured diffuse auroral patch was stable for a few tens of minutes and slowly drifted azimuthally. The high correlation of waves and auroras indicates that the structured diffuse auroral pattern reflects the spatial distribution of whistler-mode waves and ambient plasma density in space. The enhanced density measured by the spacecraft is quasi-spatial and contributes to enhanced growth of whistler-mode waves.

Citation: Nishimura, Y., et al, (2013), Structures of dayside whistler-mode waves deduced from conjugate diffuse aurora, *J. Geophys. Res. Space Physics*, *118*, 664–673, doi:10.1029/2012JA018242.

1. Introduction

[2] Chorus is a common, naturally occurring type of magnetospheric whistler-mode waves. It is characterized by discrete frequency spectra, showing rising or falling tones with durations of the order of ~0.1–1 s [*Burtis & Helliwell*, 1969]. Enhancements of anisotropic electrons in the plasma sheet are responsible for generating chorus [*Tsurutani & Smith*, 1974; *Burton*, 1976; *Kennel & Petschek*, 1966; *Omura et al.*, 2009]. While intense chorus can occur in the post-midnight and dawn sectors, moderate chorus activity extends to the dayside [*Burtis & Helliwell*, 1976; *Meredith et al.*, 2001; *Li et al.*, 2009]. The occurrence frequency of the dayside chorus is as high as in post-midnight-dawn [*Koons & Roeder*, 1990]. Interestingly, quiet time chorus is predominantly seen on the dayside [*Li et al.*, 2009; *Spasojevic & Inan*, 2010], while almost disappearing on the nightside [*Tsurutani & Smith*, 1977; *Meredith et al.*, 2001; *Li et al.*, 2009]. The persistence of dayside chorus during all levels of geomagnetic activity suggests that dayside chorus is driven not only by injection of anisotropic electrons drifting from the nightside but also by additional processes that are unique to the dayside. While dayside whistler-mode waves have been extensively studied, it has been difficult to determine a nearly instantaneous distribution of waves and its evolution in time, which is needed to fully understand the generation of dayside chorus. The present study combines space and ground observations to provide information on the two-dimensional (2-D) structure and evolution of the waves.

[1]Department of Atmospheric and Oceanic Sciences, University of California, Los Angeles, California, USA.
[2]Department of Earth and Space Sciences, University of California, Los Angeles, California, USA.
[3]Research Institute for Sustainable Humanosphere, Kyoto University, Uji, Japan.
[4]Space Sciences Laboratory, University of California, Berkeley, California, USA.
[5]Laboratoire de Physique des Plasmas, CNRS/Ecole Polytechnique/UPMC/Paris-Sud 11, St Maur-des-Fossés, France.
[6]Institut für Geophysik und extraterrestrische Physik, Technischen Universität Braunschweig, Braunschweig, Germany.

Corresponding author: Y. Nishimura, Department of Atmospheric and Oceanic Sciences, University of California, Los Angeles, 405 Hilgard Ave., Los Angeles, CA 90095-1565, USA. (toshi@atmos.ucla.edu)

©2012. American Geophysical Union. All Rights Reserved.
2169-9380/13/2012JA018242

[3] *Li et al*. [2011] showed that part of the dayside chorus activity is associated with enhancements of ambient plasma density. Since the resonant energy decreases with increasing ambient density, the growth rate of the whistler-mode waves increases due to the increase in the resonant plasma sheet population. A correlation with ambient density has also been reported for hiss [*Koons*, 1989; *Moullard et al.*, 2002], which is another type of whistler-mode waves that has unstructured frequency spectra. While hiss is primarily seen in the plasmasphere [*Thorne et al.*, 1973], it has also been found in regions of enhanced plasma density in the dayside outer magnetosphere and plasma plumes [*Chan & Holzer*, 1976; *Kivelson*, 1976; *Hayakawa et al.*, 1986; *W. R. M. Li et al.*, 2012]. Structured density distributions act as ducts that trap and effectively amplify whistler-mode waves [*Bell et al.*, 2009; *Haque et al.*, 2011; *Chen et al.*, 2012]. These observations indicate that the ambient density structure plays a significant role in generating dayside whistler-mode waves.

[4] The correlation between electron density and whistler mode waves leads to fundamental questions regarding the properties of the enhanced plasma density: How do enhanced density regions evolve in time and what is the typical size of the enhanced density region? Can we distinguish between regions of whistler-mode waves that are driven by injected plasma from the nightside and those driven by density enhancements, which would allow us to understand what fraction of dayside whistler-mode waves is associated with density enhancements? These questions, however, cannot be easily addressed from satellite measurements alone because it is difficult to separate spatial and temporal effects.

[5] Ground-based 2-D auroral imaging is suitable for monitoring the shape and motion of diffuse aurora that is driven by precipitating electrons interacting with whistler-mode waves. However, measurements of dayside diffuse aurora are limited to the southern winter seasons and hence fewer reports exist than of nightside diffuse aurora. Nevertheless, it has been shown that the equatorward portion of the dayside aurora is dominated by diffuse aurora due to precipitating energetic electrons from the central plasma sheet [*Lorentzen & Moen*, 2000; *Sandholt et al.*, 2002; *Lorentzen et al.*, 1996]. *Ebihara et al*. [2007] showed using South Pole all-sky imager data that dayside diffuse aurora contains small-scale patches that are quasi stationary for several hours. They suggested that those patches are related to enhanced plasma density in the magnetosphere. If this is true, the density enhancements associated with whistler-mode intensifications mentioned above [*Chan & Holzer*, 1976; *Li et al.*, 2011] could be linked to such diffuse auroral structures. Furthermore, if there is such a linkage, then the shape and motion of the diffuse aurora would allow us to monitor how the ambient plasma evolves in the dayside magnetosphere, creating a remote-sensing technique to measure plasma density dynamics.

[6] It has, however, been difficult to obtain conjunctions between dayside imagers and near-equatorial satellites, which are necessary to evaluate the linkage between magnetospheric density patches, chorus, and the dayside aurora, because dayside auroral measurements are limited to polar night seasons. The THEMIS spacecraft, however, provided opportunities for finding such conjunctions, because their apogee was located on the dayside during southern winter in 2007–2009. The present study analyzes simultaneous multi-probe measurements near the magnetic equator and conjugate aurora in the southern hemisphere and demonstrates the link between intensities of whistler-mode waves in the magnetosphere and diffuse aurora in the ionosphere. We further show that the structured diffuse aurora highlights the distribution of the enhanced plasma density in the magnetosphere and discuss motion of the magnetospheric plasma that is inferred from the diffuse aurora evolution.

2. Data Set and Event Selection

[7] The aurora data we used were obtained by the all-sky imager installed at the South Pole station (−74.3° magnetic latitude (MLAT)) [*Ebihara et al.*, 2007]. Snapshots of the 557.7 nm emission, which is sensitive to energetic (~10 keV) electron precipitation, were recorded every ~44 s with a 4 s exposure. The spatial resolution of the CCD camera is 512 × 512 pixels. The imager capability of measuring dayside diffuse aurora including small-scale (~20 km) features has been demonstrated by *Ebihara et al*. [2007]. Magnetic coordinates of the imager data were obtained by projecting data to the 110 km altitude plane.

[8] We surveyed conjunction events during southern polar nights in 2008 and 2009, when the apogees of the THEMIS probes [*Angelopoulos*, 2008] were located on the dayside in the southern winter seasons. We required that the nominal spacecraft footprints using the T01 magnetic field model [*Tsyganenko*, 2002] were located within the imager field of view (FOV), the sky conditions were favorable for measuring diffuse aurora without significant clouds or moonlight, and that THEMIS measured whistler wave activity in the filter bank (FBK) data [*Cully et al.*, 2008] from the electric [*Bonnell et al.*, 2008] and magnetic field [*Le Contel et al.*, 2008] instruments outside the plasmasphere. The T01 model was used only for roughly estimating the spacecraft footprints, and the possible footprints ware calculated independently from a cross-correlation analysis [*Nishimura et al.*, 2010]. Since the frequency and time resolution of FBK is limited (4 s cadence and six frequency bins), we do not distinguish between hiss and chorus but call all waves in a range of 0.05–1 electron cyclotron frequency (f_c) (obtained from the magnetic field instrument) [*Auster et al.*, 2008] whistler-mode waves. Electron distributions were measured by the electrostatic analyzer (ESA) [*McFadden et al.*, 2008] and solid state telescope (SST), and total plasma density was inferred from the spacecraft potential using the method proposed by *Mozer* [1973] and *Pedersen et al.* [1998]. We validated the accuracy of the density from the spacecraft potential by comparing with the density moment from ESA when radiation belt contamination is small.

[9] We found 15 conjunctions during 7 days (27 July, 4 and 5 August in 2008 and 9, 13, 14 and 22 August in 2009), all of which occurred when the probes were north of but close to the magnetic equator based on the dipole latitude and the direction of the radial component of the magnetic field. If the wave-particle interactions occur near the magnetic equator, the THEMIS-South Pole pair is suitable for studying the wave-particle interaction because it is able to image aurora caused by electrons precipitating toward the southern hemisphere that interact with waves propagating northward, assuming a first-order cyclotron resonant interaction. We, however, do not rule out the possibility that the measured waves

originate from a mid-latitude source, although the measurements were performed close to the equator.

[10] We show two representative cases in sections 3.1 and 3.2, and all events are compiled in a statistical study in section 3.3. Aurora data are shown in four different formats: The 2-D images are presented in magnetic coordinates at 110 km. Keograms and ewograms [*Donovan et al.*, 2006] are time series of auroral intensity along constant longitudes and latitudes. The keograms used for wave-aurora comparisons are also intensity cuts in the north-south direction but are given in the T01 footprint-centered coordinates. Namely, the imager data were converted to the magnetic coordinates that are relative to the T01 footprints and then sliced to make the keograms, in order to remove the spacecraft motion effects over 1–2 h of the conjunction periods. The coordinates relative to the T01 footprints were also used to calculate cross-correlation coefficients.

3. Results

3.1. The 13 August 2009 Event

[11] Figure 1 shows TH-D and E measurements of the waves, ambient electron density, and electron spectra. The two spacecraft were on the same orbit ~1 h apart and traversed roughly radially outward in the noon sector. The density data in the third panels indicate that the probes were initially in the plasmasphere (PS). After crossing the plasmapause at 5.5 R_E for both spacecraft (first vertical lines, here the plasmapause refers to the outermost sharp density gradient), the probes entered a region with a density that was low and smoothly decreased with radial distance. Then the density abruptly increased at the second vertical lines and fluctuated with an amplitude of up to an order of magnitude. This high-density population can be seen in the low-energy portion of the electron energy spectra. The high electron flux below ~100 eV is positively correlated with the total density. The spacecraft potential was below 12 V (not shown), indicating that the low-energy electron flux was not due to secondary electrons or photoelectrons. The energetic electron flux (>1 keV) was decreasing in time without correlating with the ambient density. These three regions of density, i.e., (1) the plasmasphere, (2) a smooth, low density region, and (3) a fluctuating density region, were detected by both probes, indicating that those are quasi spatial structures. However, the rapidly changing density fluctuations following the second vertical lines did not coincide with each other, indicating a presence of dynamical evolution within the fluctuating density region.

[12] The wave characteristics are different in the three regions. Waves in the plasmasphere can be considered as plasmaspheric hiss. The energetic electron flux was negligibly small, and thus the hiss waves were likely generated elsewhere and propagated into this region [*Bortnik et al.*, 2009]. Intense whistler-mode waves were present in the smooth low-density region. These waves extended throughout this region except just outside the plasmapause and had intensity peaks in the region of high anisotropic plasma sheet fluxes. The correlation between the wave and plasma sheet electrons indicates that the waves were generated by the anisotropic electron distributions.

[13] Whistler-mode waves in the fluctuating density region were weaker and more intermittent. The wave activity was

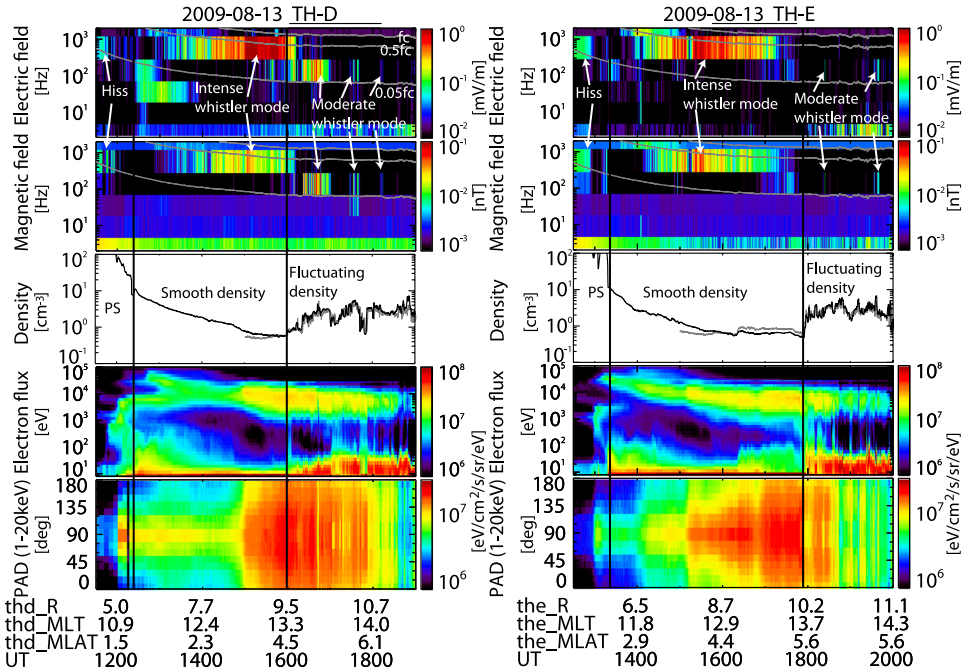

Figure 1. The TH-D and E measurements of wave electric and magnetic fields, ambient plasma density (black: inferred from the spacecraft potential, gray: ESA density moment), electron energy spectra (ESA and SST combined), and pitch angle distribution of 1–20 keV electrons on 13 August 2009. The gray lines in the wave spectra show 1.0, 0.5, and 0.05 local f_c. The vertical lines indicate the plasmapause location and the transition between the smooth and fluctuating densities. The black horizontal bars at the top are the conjunction periods with the imager.

seen in the areas of enhanced density, and the wave intensity reduced to the noise level when the density was low. In addition, the wave frequency was lower than that in the smooth low-density region. For a specified cyclotron resonant energy, the resonant frequency is inversely proportional to plasma density [*Kennel & Petschek*, 1966], which accounts for the reduced frequency. The positive correlation between the density and wave intensity is consistent with the results of *Li et al*. [2011].

[14] No significant wave activity in the electric field above the gyro frequency was detected. Thus the electron cyclotron harmonic (ECH) waves during this period were negligibly weak. This is consistent with a low statistical occurrence of ECH waves on the dayside [*Ni et al.*, 2011a] and indicates that the measured whistler-mode waves are the unique candidate for waves that could resonate with plasma sheet electrons, leading to electron precipitation toward the ionosphere.

[15] Figure 2 presents the imager data during the spacecraft-imager conjunctions, which are indicated by the black horizontal bars at the top of Figure 1. Magnetic south is on top, and east (duskside) is to the left. The red line indicates the magnetic noon meridian. A keogram and ewogram are also given in Figures 3d–3f. The measured aurora was dominated by diffuse aurora except for a rayed discrete arc at −76° to −77° MLAT. A diffuse auroral band that was aligned azimuthally was present at approximately −70° to −72° MLAT (indicated by the magenta curves in Figure 2). The keogram and ewogram (Figures 3d and 3f) show that this diffuse auroral band extends over 2 h MLT and was present for >3 h. The diffuse aurora poleward of it (approximately −72° to −74° MLAT) was fainter and more structured with a scale size of ~100–200 km. In contrast to the quasi steady nature of the diffuse aurora band, the structured diffuse aurora evolved dynamically by changing its shape and location. The red arrows in Figures 2a–2c mark three different patches slowly drifting dawnward (i.e., toward the right of the figure) and decaying in intensity. The same sequence occurred for another three patches shown in Figures 2d–2f. These azimuthal motions are also illustrated in Figure 3e as tilted traces of luminous structures. The patches at ≲12.5 h MLT (Figures 2a–2c) propagated dawnward with a speed of ~0.05 MLT/min, while the patches at ≳12.5 h MLT (Figures 2d–2f) were almost stagnant or slowly propagated duskward at ~0.01 MLT/min. The existence of patches drifting dawnward suggests that the patch motion is not due to the magnetic drift of plasma sheet electrons, which is directed duskward.

[16] Figures 3g and 3h show 2-D cross-correlation coefficients of the auroral intensity and wave electric field intensity measured on TH-D and E that were integrated over the top three frequency channels (see Figure 4). We use magnetic coordinates relative to the T01 footprint, and the axes are inverted in order to make comparisons with the 2-D images easier. For each of the conjunctions indicated by the horizontal bars at the top of Figure 1, the entire conjunction period was used for calculating the correlation coefficient. The grid size is 0.5° MLAT and 1.5° magnetic longitude (MLON). Since we integrate over a long time for increasing statistical significance, the correlation map does not represent diffuse auroral structure at a particular time but integrates all structures passing each grid. The SYMH, AU, and AL indices during this period were quite low, and the IMF B_z was close to zero

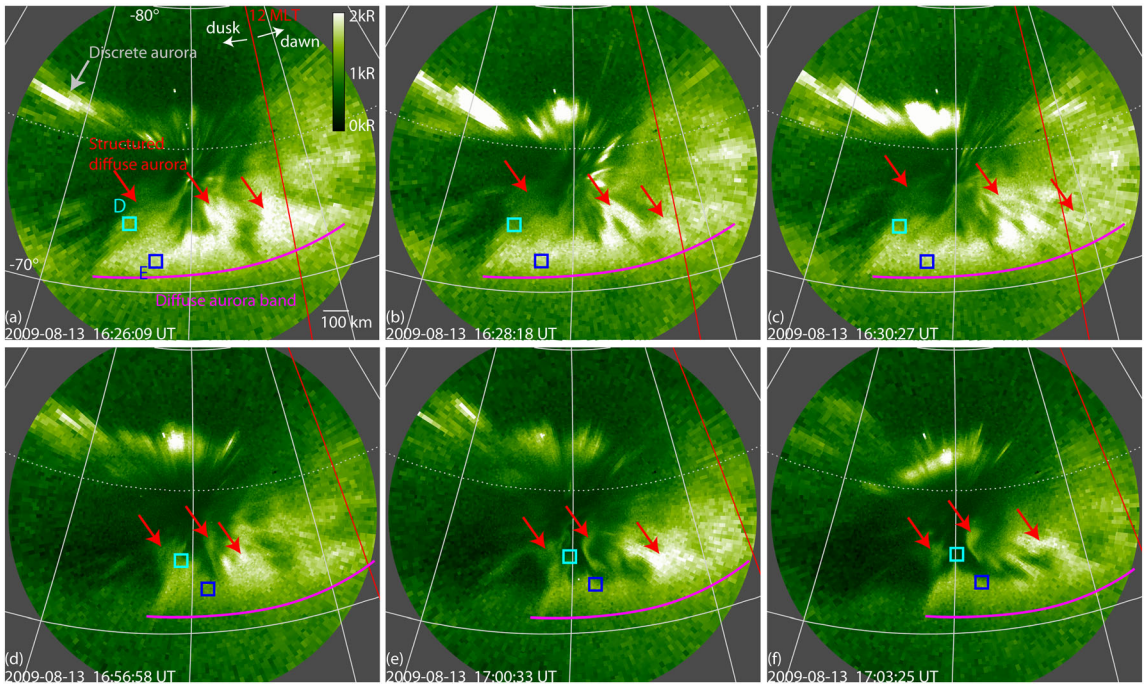

Figure 2. South Pole all-sky imager snapshots at 557.7 nm wavelength. Magnetic south is on top, and east (duskside) is to the right. The TH-D and E footprints using T01 are drawn in cyan and blue squares. The solid latitude and longitude contours are given in every 10° and 15°. The magnetic noon is indicated by the red line.

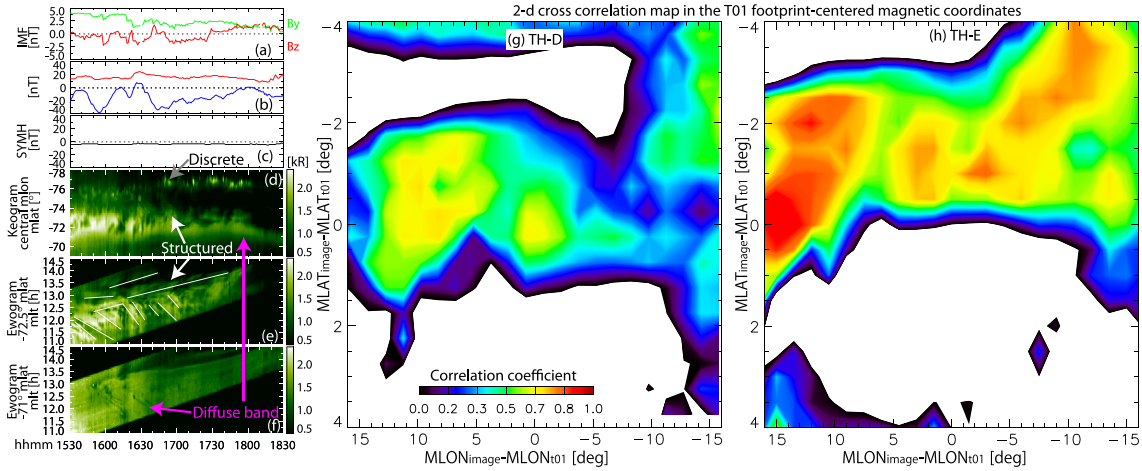

Figure 3. (a–f) The IMF B_y and B_z, AU and AL, SYMH, auroral keogram at the imager central meridian, and ewograms at −72.5° and −71° MLAT. The white lines in Figure 3e trace motion of diffuse auroral patches. (g–h) The 2-D maps of cross-correlation coefficients of wave and aurora intensities in the T01 footprint-centered coordinates.

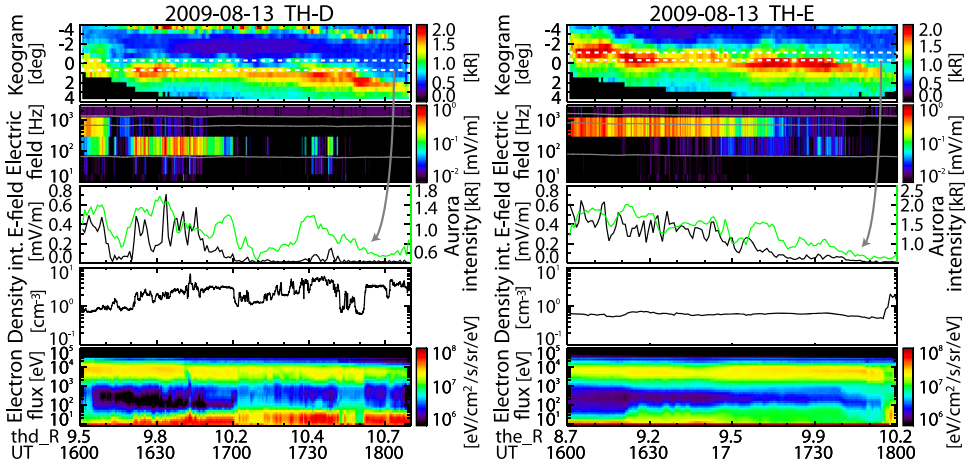

Figure 4. Aurora and spacecraft data during the conjunctions. The first row shows auroral keograms at the highest cross-correlation meridian. The latitude is given relative to that of the T01 model. The aurora intensity in the white dashed box is given by the green lines in the third row. The black line in the third row is the wave intensity integrated over the top three frequency channels. The rest of the rows are blowups of those in Figure 1.

with small perturbations (Figures 3a–3c), indicating that this conjunction occurred during a relatively quiet time.

[17] The correlation coefficients of the aurora and whistler wave are remarkably high. The maximum values reached 0.72 and 0.92 for TH-D and E. Such high correlation provides evidence that the whistler-mode waves measured by THEMIS scattered plasma sheet electrons and lead to diffuse auroral emissions. The high-correlation regions for both TH-D and E were mostly confined to −2°–0° MLAT, suggesting that the real footprint latitudes were close to those predicted by T01. The longitudinal deviation for TH-D was confined to approximately −2°–12° MLON, while the high-correlation region for TH-E extends over a wide longitude range possibly due to the azimuthally extended diffuse aurora band. Thus the longitudinal accuracy for the TH-E mapping could not be determined. Nevertheless, based on the latitudinal mapping accuracy, TH-D and E were inferred to be along the field lines of the structured diffuse aurora and diffuse aurora band, respectively, for most of the time of the conjunction.

[18] Figure 4 compares wave and auroral measurements during the conjunction. The keograms shown in the first row are a north-south cut along the meridian containing the highest correlation location (Figures 3g and 3h) and are given in the T01 footprint-centered coordinates. The auroral intensities in the white dashed boxes are shown in green in the third row. The electric field intensity integrated over the highest three frequency channels, which was used for the cross-correlation analysis, is shown in black in the third row. The other rows are blowups of those in Figure 1.

[19] The TH-D was in the fluctuating density region during the conjunction. The plasma density was enhanced during 1620–1700 and 1715–1740 UT, and the wave

activity was detected during the high-density periods. The auroral intensity was positively correlated with the wave amplitude: The peaks in the auroral intensity at 1600–1610, 1620–1700, and 1730 UT coincided with the wave intensifications. The correlation coefficient (0.72) is remarkably high, although the correlation is not perfect particularly on short time scales. TH-E was located ~1 R_E closer to the Earth and in the smooth low-density region. The wave intensity was elevated and slowly decayed as the probe moved outward. The auroral intensity in the highest correlation region also decreased in time with the cross-correlation coefficient of 0.92.

[20] The high correlations seen simultaneously in both spacecraft-aurora pairs strongly indicate that the diffuse aurora at the highest correlation location is driven by precipitating electrons that interact with whistler-mode waves. The fact that the other modes of waves such as ECH waves were negligibly small also supports the above hypothesis that the whistler-mode waves are responsible for the electron scattering. Moreover, since the TH-D and E footprints are identified to be within the structured and banded diffuse aurora regions, respectively, the diffuse aurora band is associated with the intense whistler-mode waves in the low density region outside the plasmapause, and the structured diffuse aurora reflects the enhanced and fluctuating density outside the low density region. While the spacecraft measurements do not distinguish if the density enhancements are spatial or temporal, the propagation of the structured diffuse aurora indicates that the enhanced densities are spatial and slowly drifted westward. The dawnward-moving diffuse auroral patches are likely due to the motion of ambient plasma by E × B drifts [*Nakamura & Oguti*, 1987; *Ebihara et al.*, 2007] rather than by magnetic drifts, although we cannot directly confirm this hypothesis from the THEMIS observations due to the very small drift speed. If we simply map the diffuse aurora structure toward the magnetosphere, the density structures are inferred to extend over ~3000–6000 km.

3.2. The 22 August 2009 Event

[21] Figures 5–8 present another event that supports the results described above. The spacecraft trajectories are almost the same as in the previous event. Both probes measured the three regions of the whistler-mode waves and plasma density as shown in Figure 5: from low to high *L*-shells, hiss in the plasmasphere, intense whistler-mode waves in the smooth low density, and moderate whistler-mode waves in the fluctuating high density. The two-spacecraft measurements demonstrate that this is a quasi-spatial profile, while the rapidly changing density fluctuations evolved between the probe passages, indicating a presence of variations an ~1 h time scale. Like in the previous event, the whistler-mode waves in the smooth low density are likely driven by the anisotropic energetic electrons, based on the correlation with the energetic electron flux. The waves in the fluctuating density are correlated with the density enhancements, which can also be seen in the low-energy portion of the electron energy spectra, and is consistent with the waves generated by the lower resonant energy relative to that in the surrounding plasma. Moderate wave activity in the fluctuating density region can be seen at lower frequencies than those in the smooth density regions.

[22] The auroral image snapshots in Figure 6 show structured diffuse auroral patches at −71° to −74° MLAT as indicated by the red arrows. The patches were more quasi-stationary and were identifiable for longer times than in the previous event. Representative patches are marked in Figures 6a, 6c, 6d, and 6f. The ewogram in Figure 7e indicates that those patches roughly stayed at the same MLTs for a few tens of minutes. Unstructured diffuse aurora was located equatorward of the structured aurora. Its equatorward edge could not be determined due to the dayglow contamination.

[23] The cross-correlation coefficients in Figures 7g and 7h were calculated in the same way as in Figure 3 and are lower than those in the previous event probably because the wave and aurora are weaker. While peaks in the correlation coefficients were localized in space, the real footprints could not be uniquely determined due to the presence of multiple peaks. However, the wave-aurora comparisons in the third panels of Figure 8 show moderate correlations between the peaks of waves and auroras, where the auroral intensities were obtained from the highest correlation locations near the left edge of Figure 7g and near the center of Figure 7h. Particularly for TH-E (right column of Figure 8), the distinct density enhancements at 1550–1610 and 1630–1634 UT are well correlated with the wave and auroral intensifications, while the high energy electron flux was almost constant. Both the density and electron flux changed for TH-D during the wave and auroral intensifications (left column of Figure 8) and thus the cause of each wave enhancement cannot be uniquely determined. However, the density effect on the overall intensifications is quite clear from Figure 5. Moreover, the auroras near the T01 footprints of the spacecraft were dominated by the diffuse auroral patches. Thus the real footprints are likely located in this auroral region. The high degree of correlation among diffuse aurora luminosity, whistler-mode intensity, and ambient density again indicates that the structured diffuse auroral pattern reflects the distribution of the waves and that the motion of diffuse auroral patches is due to convection of low energy magnetospheric plasma.

3.3. Statistical Wave-Aurora Intensity Relation

[24] We investigated the wave-aurora correlation for all 15 conjunction events and present the results in Figure 9. We first created the cross-correlation coefficient maps and determined the highest correlation locations for all events. Then the auroral intensities at those locations were combined and plotted in this figure as a function of the whistler-mode intensity. The correlation can be seen even after combining all cases and roughly follows a linear regression curve. The L^*-shell [*Roederer*, 1970] (using the *Tsyganenko* [1995] model) dependence as color coded further shows that the wave and aurora at inner L^* tend to be stronger. The bottom panel is color coded by the different plasma density structures. Most of the red and blue dots on this panel correspond to the same colors in the top panel, indicating that the intense waves and auroras at the inner L^* occur along the field lines with a smooth, low density and that the weak waves and auroras at the outer L^* are found along field lines of fluctuating density. This relation is consistent with the case studies in sections 3.1 and 3.2 and seems common within the conjunction events we obtained.

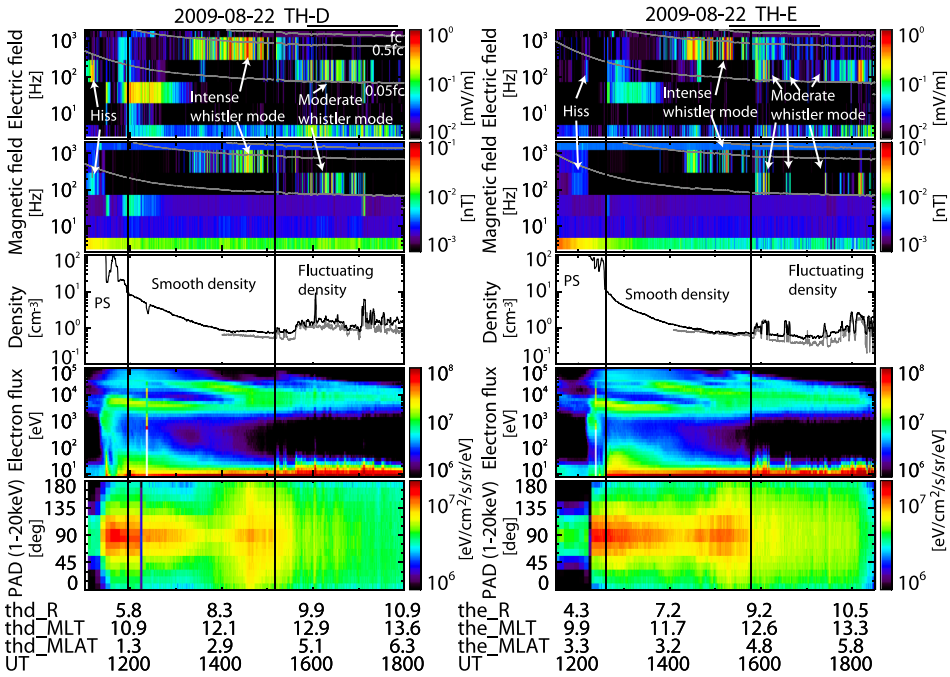

Figure 5. The TH-D and E data on 22 August 2009. The format is the same as in Figure 1.

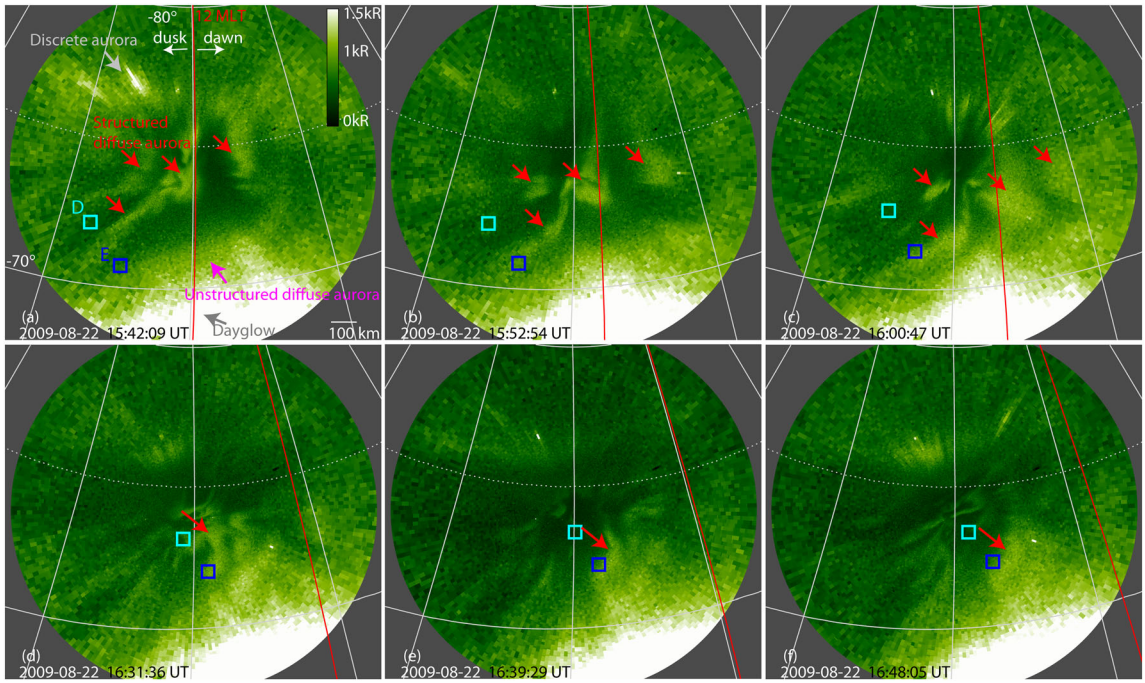

Figure 6. Imager data during the 22 August 2009 conjunction event. The format is the same as in Figure 2. The bright emission near the northern edge of the FOV is dayglow contamination.

[25] The statistical correlation suggests that the whistler-mode wave intensity in the magnetosphere strongly controls the diffuse aurora intensity, consistent with previous findings by *Thorne et al.* [2010] and *Ni et al.* [2011b]. We note, however, that we did not consider various factors that could affect the wave-aurora intensity relation. The diffusion coefficient, electron flux, and atmospheric density should all be considered in estimating the electron precipitating flux and auroral emission rates, and those effects might be the cause of some of the scatter of the data points around a regression line.

4. Conclusion

[26] We investigated a number of coordinated observations by the THEMIS probes and the South Pole all-sky imager on the dayside during the southern winter seasons (i.e., when the

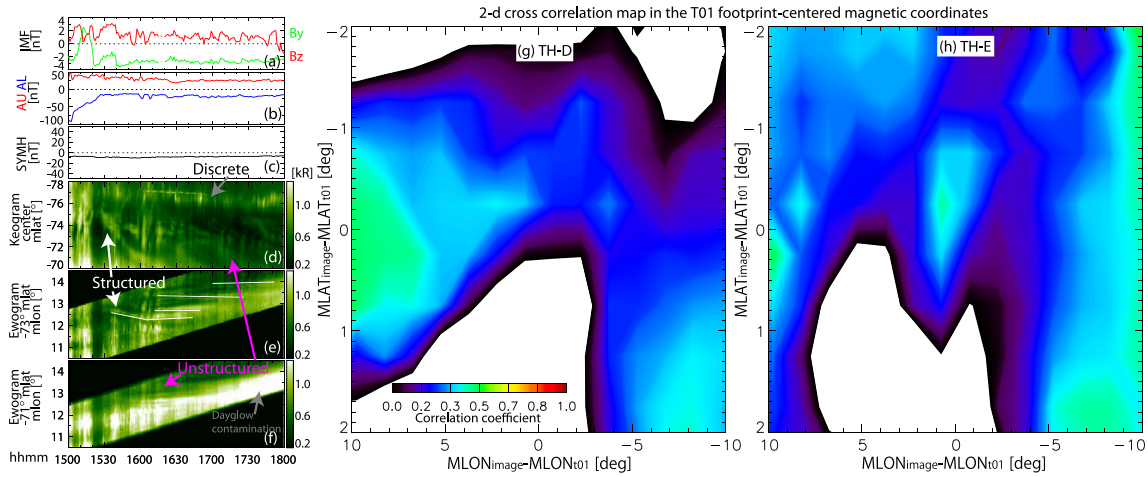

Figure 7. Solar wind and geomagnetic conditions, auroral time series, and cross correlation maps. The format is the same as in Figure 3.

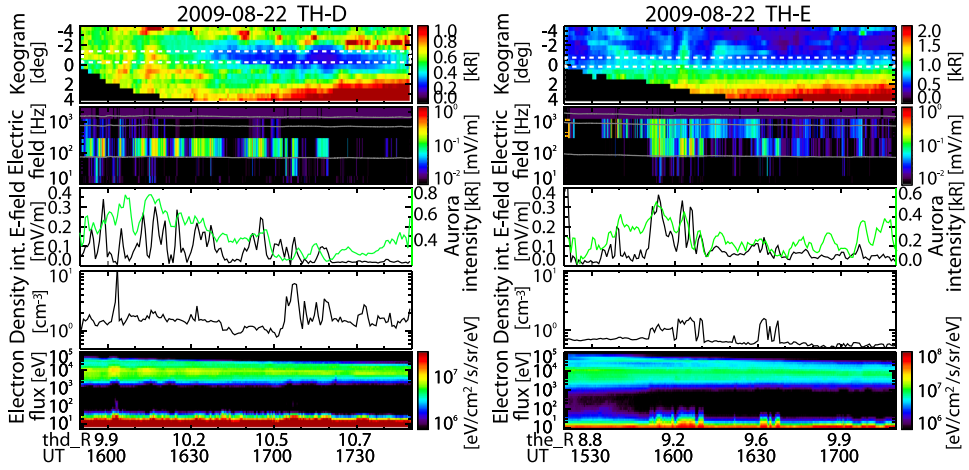

Figure 8. Wave-aurora comparison. The format is the same as in Figure 4.

imager was in darkness). The THEMIS spacecraft measured two distinct regions of the plasma density and wave activity outside the plasmasphere: intense whistler-mode waves in smooth low density and moderate whistler-mode waves correlating with a fluctuating, enhanced plasma density. The correlation between the wave amplitude and density indicate that the whistler-mode waves correlating with the density are driven by reduced resonant energy in spite of lower plasma sheet fluxes, while the whistler-mode waves in the smooth low density are generated by enhanced population of anisotropic plasma sheet electrons. The enhanced density is characterized by enhanced fluxes of low-energy (<100 eV) electrons, coexisting with plasma sheet electrons (>keV). This particle spectral feature resembles the mixing region of plasmas originating from the magnetosphere and magnetosheath [*Hasegawa et al.*, 2003; *Øieroset et al.*, 2008]. In fact, the magnetopause was located within 1.5 R_E of the probes (based on the *Shue et al.* [1998] model) when the high density plasma was detected in Figures 1 and 5. While it is beyond the scope of the present study to seek the origin of the enhanced density, magnetosheath electrons could be a candidate for the source population that leads to the density fluctuations in the outer magnetosphere and associated modulations of whistler-mode intensities.

[27] The conjugate auroral measurements detected two types of dayside diffuse aurora: (i) an azimuthally elongated diffuse auroral band and (ii) a structured diffuse aurora. The structured diffuse aurora is located poleward of the diffuse auroral band and consists of auroral patches of ~100–200 km in size that are stable for a few tens of minutes. Cross-correlation analyses of the wave and auroral intensities showed that the diffuse auroral intensity near the T01 footprint latitude of the spacecraft is correlated with the whistler-mode wave intensity, indicating that the T01 model represents the geometry of the ambient magnetic field well within an accuracy of ~1° MLAT. This link between the ground and space phenomena leads us to conclude that the dayside whistler-mode waves drive the dayside diffuse aurora and that the diffuse auroral pattern reflects the distribution of whistler-mode waves that is determined by the density distribution of the low-energy plasma. This direct association between the auroral patches and magnetospheric density enhancements support earlier suggestions regarding this link from ground-based observations alone [*Ebihara et al.*, 2007].

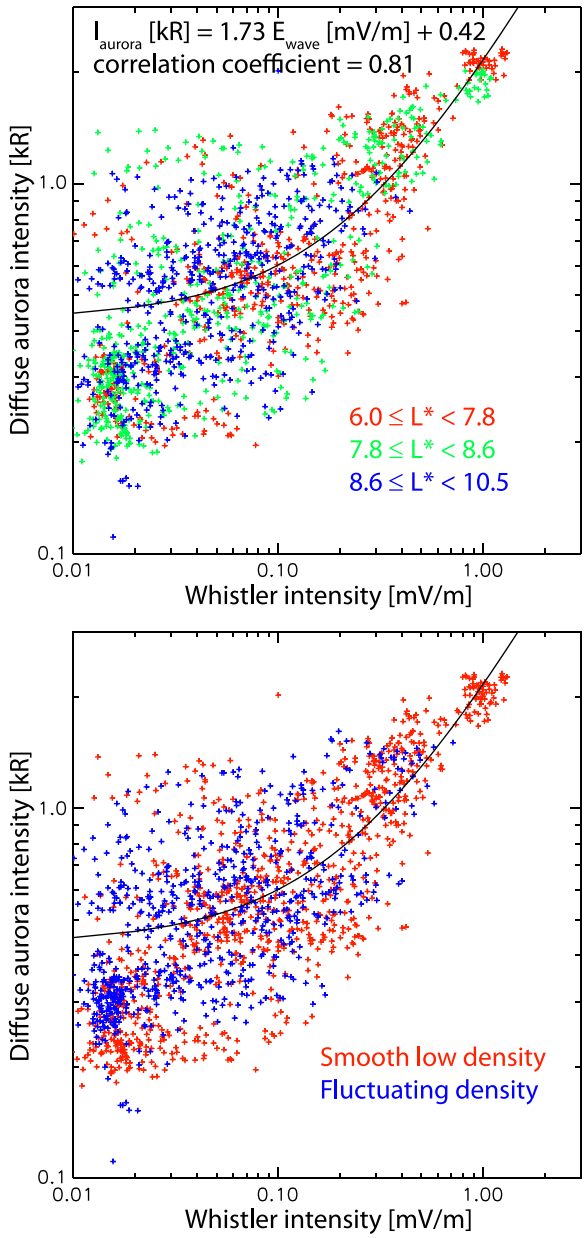

Figure 9. Scatter plots of wave and aurora intensities. The top panel is color coded according to L^*, and the bottom panel is parameterized by the different density regimes. The black line is the linear regression curve.

[28] The well-defined shape of the structured diffuse aurora allows tracing motion of the diffuse auroral patches. Some patches were found to drift dawnward or stayed at constant MLTs. Those motions cannot be explained by the magnetic drift of plasma sheet electrons. Based on the correlation between the patches and low-energy plasma density, the patch motion is likely due to the $E \times B$ drift in the magnetosphere.

[29] **Acknowledgments.** This work was supported by NASA contract NNX09AI06G, NAS5-02099, NNX12AJ57G, NNX11AD75G, NNX12AD12G, and NSF grants AGS-1042255, AGS-0840178, ATM 0802843 and AGS-1101903. The South Pole imager is supported by NSF grant ANT-0638587. The authors thank J. McFadden for the ESA data, the ONERA library for providing the tools to calculate L^*, the World Data Center for Geomagnetism, Kyoto for providing AU, AL, and SYMH indices, and the Space Physics Data Facility at the NASA Goddard Space Flight Center for providing the OMNI2 data.

References

Angelopoulos, V. (2008), The THEMIS Mission, *Space Sci. Rev.*, p. 47.
Auster, H., et al. (2008), The THEMIS fluxgate magnetometer, *Space Sci. Rev.*, p. 135.
Bell, T. F., U. S. Inan, N. Haque, and J. S. Pickett (2009), Source regions of banded chorus, *Geophys. Res. Lett.*, *36*, L11101.
Bonnell, J. W., et al., (2008), The electric field instrument (EFI) for THEMIS, *Space Sci. Rev.*, *141*, 1-4, pp. 303–341.
Bortnik, J., W. Li, R. M. Thorne, V. Angelopoulos, C. Cully, J. Bonnell, O. Le Contel and A. Roux (2009), An observation linking the origin of plasmaspheric hiss to discrete chorus emissions, *Sci.*, *324*, 5928, 775–778.
Burtis, W. J., and R. A. Helliwell (1969), Banded chorus—A new type of VLF radiation observed in the magnetosphere by OGO 1 and OGO 3, *J. Geophys. Res.*, *74*(11), 3002–3010.
Burtis, W.J., and R.A. Helliwell (1976), Magnetospheric chorus: Occurrence patterns and normalized frequency, *24*, 11, 1007.
Burton, R. K. (1976), Critical electron pitch angle anisotropy necessary for chorus generation, *J. Geophys. Res.*, *81*(25), 4779–4781.
Chan, K.-W., and R. E. Holzer (1976), ELF hiss associated with plasma density enhancements in the outer magnetosphere, *J. Geophys. Res.*, *81*(13), 2267–2274.
Chen, L., R. M. Thorne, W. Li, J. Bortnik, D. Turner, and V. Angelopoulos (2012), Modulation of plasmaspheric hiss intensity by thermal plasma density structure, *Geophys. Res. Lett.*, *39*, L14103.
Cully, C. M., R.E. Ergun, K. Stevens, A. Nammari, and J. Westfall (2008), The THEMIS digital fields board, *Space Sci. Rev.*, *141*, 343–355.
Donovan, E., et al. (2006), The THEMIS all-sky imaging array—System design and initial results from the prototype imager, *J. Atmos. Sol. Terr. Phys.*, *68*, 13, 1472–1487.
Ebihara, Y., Y.-M. Tanaka, S. Takasaki, A. T. Weatherwax, and M. Taguchi (2007), Quasi-stationary auroral patches observed at the South Pole station, *J. Geophys. Res.*, *112*, A01201.
Haque, N., U. S. Inan, T. F. Bell, J. S. Pickett, J. G. Trotignon, and G. Facskó (2011), Cluster observations of whistler mode ducts and banded chorus, *Geophys. Res. Lett.*, *38*, L18107.
Hasegawa, H., M. Fujimoto, K. Maezawa, Y. Saito, and T. Mukai (2003), Geotail observations of the dayside outer boundary region: Interplanetary magnetic field control and dawn-dusk asymmetry, *J. Geophys. Res.*, *108*, 1163.
Hayakawa, M., N. Ohmi, M. Parrot, and F. Lefeuvre (1986), Direction finding of ELF hiss emissions in a detached plasma region of the magnetosphere, *J. Geophys. Res.*, *91*(A1), 135–141.
Kennel, C. F., and H. E. Petschek (1966), Limit on stably trapped particle fluxes, *J. Geophys. Res.*, *71*, 1.
Kivelson, M. G. (1976), Instability phenomena in detached plasma regions, *J. Atmos. Terr. Phys.*, *38*, 1115.
Koons, H. C. (1989), Observations of large-amplitude, whistler mode wave ducts in the outer plasmasphere, *J. Geophys. Res.*, *94*, 15,393–15,397.
Koons, H.C., J.L. Roeder (1990), A survey of equatorial magnetospheric wave activity between 5 and 8 RE, 38, 10, 1335.
Le Contel et al. (2008), First results of the THEMIS search coil magnetometers, *Space Sci. Rev.*, *141*, Issue 1-4, pp. 509–534.
Li, W., et al. (2009), Global distribution of whistler-mode chorus waves observed on the THEMIS spacecraft, *Geophys. Res. Lett.*, *36*, L09104.
Li, W., J. Bortnik, R. M. Thorne, Y. Nishimura, V. Angelopoulos, and L. Chen (2011), Modulation of whistler mode chorus waves: 2. Role of density variations, *J. Geophys. Res.*, *116*, A06206.
Li, W., R. M. Thorne, J. Bortnik, X. Tao, and V. Angelopoulos (2012), Characteristics of hiss-like and discrete whistler-mode emissions, *Geophys. Res. Lett.*, *39*, l18106, doi:10.1029/2012GL053206.
Lorentzen, D. A., C. S. Deehr, J. I. Minow, R. W. Smith, H. C. Stenbaek-Neielsen, F. Sigernes, R. L. Arnoldy, and K. Lynch (1996), SCIFER—Dayside auroral signatures of magnetospheric energetic electrons, *Geophys. Res. Lett.*, *23*(14), 1885–1888.
Lorentzen, D. A., and J. Moen (2000), Auroral proton and electron signatures in the dayside aurora, *J. Geophys. Res.*, *105*(A6), 12,733–12,745.
J. P. McFadden, C. W. Carlson, D. Larson, J. Bonnell, F. Mozer, V. Angelopoulos, K.-H. Glassmeier and U. Auster (2008), THEMIS ESA first science results and performance issues, *Space Sci. Rev.*, *141*, 1-4, 477–508.
Meredith, N. P., R. B. Horne, and R. R. Anderson (2001), Substorm dependence of chorus amplitudes: Implications for the acceleration of electrons to relativistic energies, *J. Geophys. Res.*, *106*(A7), 13,165–13,178.

Moullard, O., A. Masson, H. Laakso, M. Parrot, P. Décréau, O. Santolik, and M. Andre (2002), Density modulated whistler mode emissions observed near the plasmapause, *Geophys. Res. Lett.*, *29*(20), 1975.

Mozer, F. S. (1973), Analysis of techniques for measuring DC and AC electric fields in the magnetosphere, *Space Sci. Rev.*, *14*(2), 272–313.

Nakamura, R., and T. Oguti (1987), Drifts of auroral structures and magnetospheric electric fields, *J. Geophys. Res.*, *92*(A10), 11,241–11,247.

Ni, B., R. Thorne, J. Liang, V. Angelopoulos, C. Cully, W. Li, X. Zhang, M. Hartinger, O. Le Contel, and A. Roux (2011a), Global distribution of electrostatic electron cyclotron harmonic waves observed on THEMIS, *Geophys. Res. Lett.*, *38*, L17105.

Ni, B., R. M. Thorne, N. P. Meredith, R. B. Horne, and Y. Y. Shprits (2011b), Resonant scattering of plasma sheet electrons leading to diffuse auroral precipitation: 2. Evaluation for whistler mode chorus waves, *J. Geophys. Res.*, *116*, A04219.

Nishimura, Y., et al. (2010), Identifying the Driver of Pulsating Aurora, *Science*, *330*, 6000, 81–84.

Øieroset, M., et al. (2008), THEMIS multi-spacecraft observations of magnetosheath plasma penetration deep into the dayside low-latitude magnetosphere for northward and strong By IMF, *Geophys. Res. Lett.*, *35*, L17S11.

Omura, Y., M. Hikishima, Y. Katoh, D. Summers, and S. Yagitani (2009), Nonlinear mechanisms of lower-band and upper-band VLF chorus emissions in the magnetosphere, *J. Geophys. Res.*, *114*, A07217.

Pedersen, A., F. Mozer, and G. Gustafsson (1998), Electric field measurements in a tenuous plasma with spherical double probes, in Measurement Techniques in Space Plasmas: Fields, Geophys. Monogr. Ser., vol. *103*, edited by J. Borovsky, R. Pfaff, and A. Young, pp. 1–12, AGU, Washington, D. C.

Roederer, J. G. (1970), Dynamics of Geomagnetically Trapped Radiation, Springer-Verlag Berlin, Heidelberg.

Sandholt, P. E., W. F. Denig, C. J. Farrugia, B. Lybekk, and E. Trondsen (2002), Auroral structure at the cusp equatorward boundary: Relationship with the electron edge of low-latitude boundary layer precipitation, *J. Geophys. Res.*, *107*(A9), 1235.

Shue, J.-H., et al. (1998), Magnetopause location under extreme solar wind conditions, *J. Geophys. Res.*, *103*(A8).

Spasojevic, M., and U. S. Inan (2010), Drivers of chorus in the outer dayside magnetosphere, *J. Geophys. Res.*, *115*, A00F09.

Thorne, R. M., E. J. Smith, R. K. Burton, and R. E. Holzer (1973), Plasmaspheric Hiss, *J. Geophys. Res.*, *78*(10), 1581–1596.

Thorne, R. M., B. Ni, X. Tao, R. B. Horne, and N. P. Meredith (2010), Scattering by chorus waves as the dominant cause of diffuse auroral precipitation, *Nature*, *467*, 934 – 936.

Tsurutani, B. T., and E. J. Smith (1974), Postmidnight chorus: A substorm phenomenon, *J. Geophys. Res.*, *79*(1), 118–127.

Tsurutani, B. T., and E. J. Smith (1977), Two types of magnetospheric ELF chorus and their substorm dependences, *J. Geophys. Res.*, *82*(32), 5112–5128.

Tsyganenko, N. A. (1995), Modeling the Earth's magnetospheric magnetic field confined within a realistic magnetopause, *J. Geophys. Res.*, *100*, 5599–5612.

Tsyganenko, N. A. (2002), A model of the near magnetosphere with a dawn-dusk asymmetry 1. Mathematical structure, *J. Geophys. Res.*, *107*, 1179.